

Chapter 2

Mechanical Stress Order of Grain Boundaries

The mechanical aspect is particularly important for understanding the grain boundary behaviour during plastic deformation or recrystallization, both processes involving interactions between planar and linear defects.

Two types of mechanical approaches of the grain boundary description exist:

- The continuous Frank [1] and Bilby [2] approach describes any interface as a *surface dislocation* characterized by a *Burgers vector density* or by a second order *surface dislocation tensor*. This approach is analogous to the elegant theory developed later by Kröner to account for the stresses, the energies and the curvatures introduced in a material under internal stress sources [3, 4].
- The discrete approach of Bollmann [5, 6] considers the presence of dislocations in the centres of the disturbed regions between the good crystalline regions. It generalizes at any grain boundary the first description of an intergranular order proposed by Read and Shockley [7]. It rests on the symmetry notions introduced in Sect. 1.2.

2.1 Continuous Approach: The Frank-Bilby Equation

Following Frank who describes the dislocation distribution in a low-angle grain boundary [1], Bilby introduces a procedure to deal with the dislocation distribution in a surface delimiting two Crystals I and II with a distortion discontinuity between them [2]:

$$\varepsilon_{ijk} n_l \beta_{sj}^I - \varepsilon_{ijk} n_l \beta_{sj}^{II} = \alpha_{ks} \quad (2.1)$$

with α_{ks} the surface dislocation tensor, k and s refer to the Burgers vector and to the dislocation line, respectively; n is the normal to the grain boundary plane pointing from grain I to grain II and ε_{ijk} is the permutation tensor ($\varepsilon_{ijj} = 0$).

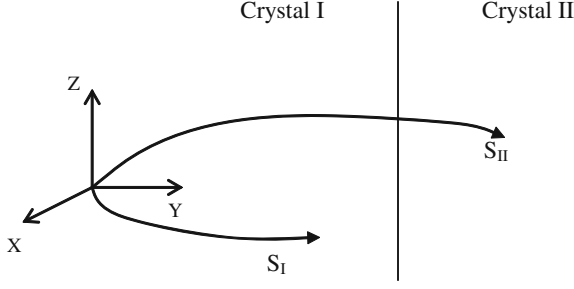


Fig. 2.1 Diagram explaining how lattices of crystals I and II are generated from a reference system XYZ by the transformations \mathbf{S}_I and \mathbf{S}_{II} , respectively

For a 2D distribution, this approach is equivalent to the Kröner generalized 3D approach in which the continuous distribution of dislocations is expressed by a dislocation density tensor $\boldsymbol{\alpha}$ related to the $\boldsymbol{\beta}$ distortion by [3, 4]:

$$\text{curl } \boldsymbol{\beta} = \boldsymbol{\alpha} \quad (2.2)$$

The expression (2.1) reformulated by Christian in matrix notation leads to the equation known as the Frank-Bilby equation that gives the Burgers vector density \mathbf{B} necessary to realise the compatibility at the interface between the crystals I and II:

$$\mathbf{B} = (\mathbf{S}_I^{-1} - \mathbf{S}_{II}^{-1}) \cdot \mathbf{X} \quad (2.3)$$

\mathbf{S}_I and \mathbf{S}_{II} are affine transformations that generate the lattices of crystals I and II starting from a reference system (Fig. 2.1), \mathbf{X} is a vector of relatively large intensity in the grain boundary plane and \mathbf{B} is the Burgers vector content of all the dislocations that are crossed by the vector \mathbf{X} . If this equation is satisfied, the grain boundary is free of long-range stresses.

Equation (2.3) is relevant for any interface but we focus here on grain boundaries.

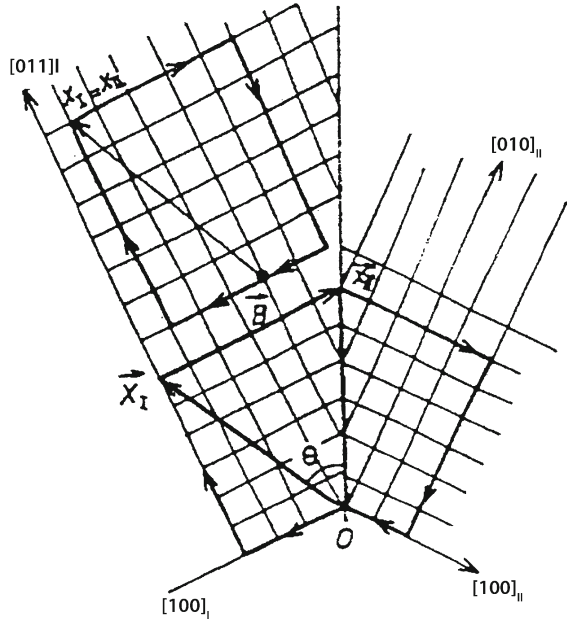
For grain boundaries in cubic materials, a simple relation links the \mathbf{S}_I and \mathbf{S}_{II} lattices to the rotation \mathbf{R} between the crystals: $\mathbf{R} = \mathbf{S}_{II} \cdot \mathbf{S}_I^{-1}$. Equation (2.3) then becomes equivalent to the 0-lattice equation in which \mathbf{I} is the identity matrix:

$$\mathbf{B} = (\mathbf{I} - \mathbf{R}^{-1})\mathbf{X} \quad (2.4)$$

In Eqs. (2.3) and (2.4), \mathbf{B} is not considered as the sum of discrete Burgers vectors belonging to the crystal translation lattice or to the DSC lattice. Such a discretization depends on the relaxation processes and is meaningless when the dislocation density is very high (Fig. 2.2).

\mathbf{B} may be determined by using the Frank circuit drawn around the grain boundary, equivalent to the Burgers circuit within the crystal (Fig. 2.2). A vector $\mathbf{X} = \mathbf{X}_{II}$, traced in the grain boundary plane and indexed in lattice II, is obtained by applying

Fig. 2.2 *Frank circuit*: a vector $X_I = X_{II}$ is drawn in lattice I, then surrounded by a *closed* circuit starting and finishing at the vector origin. The same circuit is reproduced around the grain boundary: it starts at the extremity of X_{II} (vector in the grain boundary plane obtained by the rotation θ of the vector (X_I) passes through the origin O and terminates at the extremity of X_I . This circuit displays a closure failure B given by Eq. (2.4) by substituting X for X_{II}



the rotation R to a vector X_I in lattice I:

$$X_I = R^{-1} X_{II}.$$

In the cases of symmetrical grain boundaries, if a median lattice between the two crystal lattices is considered as the reference system, then the I and II lattices are deduced from this reference by equal and opposite rotations ($\pm \theta/2$) around a ρ axis; expression (2.4) takes the well-known form of the Frank formula:

$$B = 2 \sin(\theta/2) (X \wedge \rho) \quad (2.5)$$

And provided that X is perpendicular to the rotation axis:

$$B = 2 \sin(\theta/2) |X| \quad (2.6)$$

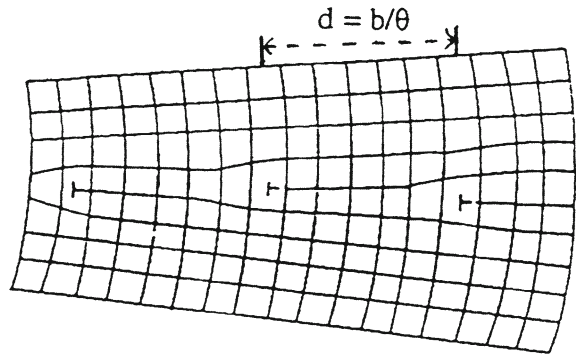
The absence of long-range stresses around the interface may be modelled by the use of two continuous distributions of dislocations with Burgers vector densities of opposite sign that cancel. One distribution may be regarded as an array of *stress-generator dislocations* or *coherency dislocations*, the other as an array of *stress-annihilator dislocations* or *anti-coherency dislocations*. For a detailed description of this approach, the reader may refer to the book by Sutton and Balluffi [8] and to the articles by Olson and Cohen [9] and Bonnet [10, 11].

2.2 Discrete Approach: The Read and Shockley Model

Studies of edge dislocation walls in a crystal, later recognised as a low-angle symmetrical tilt grain boundaries, developed about 20 years before the explicit structural model of these grain boundaries due to Read and Shockley [7]. This model links the grain boundary misorientation angle θ to the spacing d between the edge dislocations of Burgers vector b that form a periodic network in the grain boundary plane (Fig. 2.3):

$$d = \frac{b}{\theta} \quad (2.7)$$

Fig. 2.3 Scheme showing a low angle symmetrical tilt grain boundary according to Read and Shockley. The tilt axis is perpendicular to the plane of the figure



The classical Read and Shockley formula gives the intergranular energy in function of the misorientation angle, in the low-angle limit:

$$\gamma_\theta = \gamma_0 \theta (A - \ln \theta) \quad (2.8)$$

$\gamma_0 = \mu b / 4\pi(1 - \nu)$ and $A = b / 2\pi r_0$ with μ , the shear modulus, ν the Poisson coefficient and r_0 the dislocation core radius.

Equation (2.8) is easily obtained by summing the elastic energies of the N edge dislocations (of unit length) contained in a unit area of the grain boundary ($N = 1/d$). This calculation may be done provided the dislocations are sufficiently far from each other (low θ angle) and the extension of the stress fields is equal to the distance d . This equation, initially established for $\theta < 15^\circ$, is fundamental. Indeed, after having established their model, Read and Shockley predict its relevance for high-angle grain boundaries formed by dislocations evenly spaced. In 1989, Wolf proposed an empirical extrapolation of the Read and Shockley formula for high-angle grain boundaries sharing the same mean plane, by substituting θ by $\sin \theta$ [12].

In 1947, Lacombe and Beaujard [13] revealed the existence of sub-grain boundaries in aluminium single crystals owing to the preferential etching of the crystal surface on the form of etch pit alignments. But no relationship was established between etch pits and dislocations. In 1950, Read and Shockley suggested a correlation between

their model and the previous observations. It was only in 1953 that a proper verification of the validity of the *dislocation model* for sub-grain boundaries was obtained on a germanium bicrystal by Vogel et al. [14].

2.3 Bollmann's Discrete Approach: Intrinsic Dislocations

The Bollmann approach generalizes the Read and Shockley model of *intergranular dislocations* at any grain boundary. It rests on Eqs. (1.23) and (1.24) that define the O-lattice and the O2-lattice. The term *intrinsic*, which comes from the Latin *intrinsecus*, indicates that these dislocations are inherent in the grain boundary structure that cannot exist in their absence; they actually are *structural dislocations*.

2.3.1 Primary Intrinsic Dislocations

In the O-lattice equation $(\mathbf{I} - \mathbf{R}^{-1}) \mathbf{x}_O = \mathbf{B}_m$, the \mathbf{B}_m vector may always be considered as the sum of Burgers vectors $\Sigma \mathbf{b}_m$ of crystal I (subscript m for matrix). Equations (1.23) and (1.22) for non-cubic materials may be seen as the quantified form of the Frank-Bilby Eq. (2.4) for grain boundaries in which \mathbf{x}_O is a O-lattice element. The different O elements are surrounded by Wigner-Seitz cell walls. The intersections of the grain boundary plane with these walls form the b-net; they define the lines of the geometrically necessary dislocations called *primary intrinsic dislocations* (IGBD) localized in the regions of worse fit between the two crystals. The term *primary* indicates that these dislocations account for the deviation from the first invariant of the bicrystal, i.e. the single crystal ($\theta = 0$). The term *secondary* will be used to explain the deviation from the second invariant, the CSL lattice.

The primary intrinsic dislocations possess a Burgers vector \mathbf{b}_m of the perfect crystal dislocations and form a network with the same periodicity than the O-lattice (Fig. 2.4). Their spacing decreases when the misorientation angle increases according to the formula derived from the Frank Eq. (2.3) where $|\mathbf{X}| = d$:

$$d = \frac{b_m}{2\sin\Delta\theta/2} \quad (2.9)$$

For low θ values, Eq. (2.9) is identical to the Read and Shockley expression (2.7).

The uniformly spaced distribution of the primary dislocations mathematically predicted by Eq. (2.9) is generally not respected. Indeed, a spacing between two dislocations must be physically compatible with the lattice period. Only the average spacing measured on an arrangement of several dislocations meet this formula.

Let us illustrate the application of Eq. (2.4) to the prediction of the primary dislocation content in a tilt grain boundary, then in a twist grain boundary, both displaying a small misorientation $\theta = \varepsilon$.

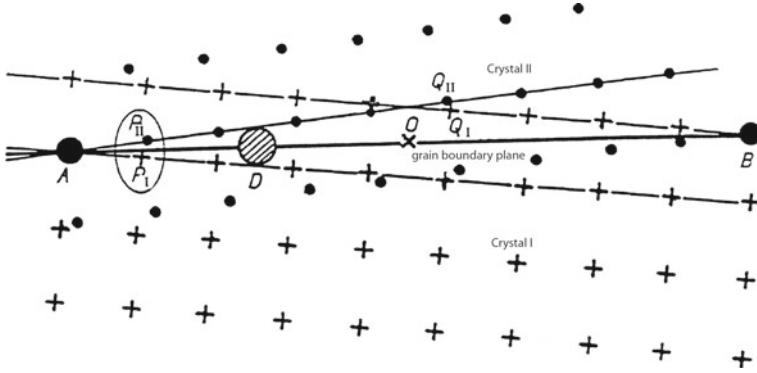


Fig. 2.4 Diagram showing the localization of the primary intrinsic dislocations in a low angle tilt grain boundary. A, B and O are nodes of the O-lattice. P_I and P_{II} (Q_I and Q_{II}) are homologous nodes assimilated to one node. D represents a region of bad fit where the primary dislocation is localized

- For a tilt grain boundary around $[011]$ with $\theta = \varepsilon$, $\cos \varepsilon \neq 1$ and $\sin \varepsilon \neq \varepsilon$. The rotation matrix \mathbf{R} between the crystals is:

$$\mathbf{R} = \begin{vmatrix} 1 & -\varepsilon & \varepsilon \\ \varepsilon & 1 & 0 \\ -\varepsilon & 0 & 1 \end{vmatrix} \quad (2.10)$$

$$\mathbf{I} - \mathbf{R}^{-1} = \begin{vmatrix} 0 & -\varepsilon & \varepsilon \\ \varepsilon & 0 & 0 \\ -\varepsilon & 0 & 0 \end{vmatrix} \quad (2.11)$$

The indices of any vector in the $(01-1)$ grain boundary plane are $[xyy]$.

The product $(\mathbf{I} - \mathbf{R}^{-1})\mathbf{X}$ in Eq.(2.4) enables to define the three components of the dislocation density vector \mathbf{B} :

$$B_x = 0 \quad B_y = \varepsilon x \quad B_z = -\varepsilon x \quad (2.12)$$

\mathbf{B} is then perpendicular to the rotation axis and to the grain boundary plane (Fig. 2.5) Furthermore:

$$\mathbf{B} = n\mathbf{b}_m \quad \text{and} \quad \mathbf{b}_m = a/2 [01-1]. \quad (2.12\text{bis})$$

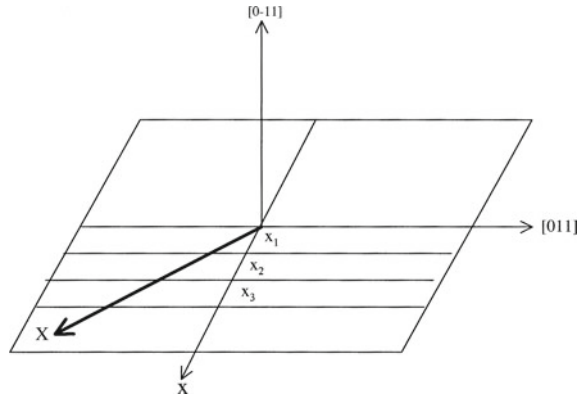
The dislocations have an edge character.

There are exact solutions for relations (2.4) only for vectors $\mathbf{X} = \mathbf{x}_0 = [xyy]$ such as:

$$x = \pm b_m/\varepsilon \quad x = \pm 2b_m/\varepsilon \quad x = \pm n b_m/\varepsilon \quad (2.13)$$

The \mathbf{X} vectors cut the intergranular dislocations along $[100]$, the dislocation lines perpendicular to $[100]$ in the grain boundary plane are parallel to $[011]$. The low-angle tilt grain boundary is well described by edge dislocations parallel to the rotation axis

Fig. 2.5 Geometry of the primary dislocation network ($b = a/2 [01-1]$) in a low angle $[011]$ tilt grain boundary



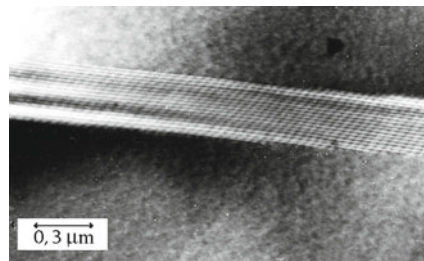
and distant from $d = b/\theta$, as predicted by Read and Shockley. In this description, the distance between the dislocations is large as $\theta = \varepsilon$ is a very small angle.

We may also describe the low angle tilt boundary by using an equivalent rotation between the crystals: $\theta = (\varepsilon + \pi)$, then $\cos(\varepsilon + \pi) \approx -1$ and $\sin(\varepsilon + \pi) = \varepsilon$. The application of the previous procedure leads to predict the occurrence of dislocations also parallel to the tilt axis but with a Burgers vector $\mathbf{b} = a [100]$. Furthermore, the distance between the dislocations is now very small ($\theta = \varepsilon + \pi$ being large). As an example, for a 2° misorientation in copper, the dislocations are distant from about 7 nm according to the first description; they may be observed by conventional transmission electron microscopy. According to the second description, the distance is about 0.12 nm and the dislocations are no longer individually distinguishable; the physical reality of this description in terms of dislocations is questionable. Rather in this case to use a continuous distribution of the deformation. It seems reasonable to consider that the dislocation structure predicted by the first description is likely to be realised. This point will be discussed further.

Figure 2.6 presents a primary dislocation network in a low-angle tilt grain boundary (2° around 111) in a iron-molybdenum alloy with a b.c.c. structure [15].

The same approach for a low-angle twist grain boundary with a $\{001\}$ plane results in a structure composed of two screw dislocation networks perpendicular to each other and with a Burgers vector $b = a/2 \langle 110 \rangle$; the distances between the dislocations

Fig. 2.6 Electronic micrograph of a $2^\circ \langle 111 \rangle$ tilt grain boundary in a Fe-1% Mo showing a primary edge dislocation network [15]



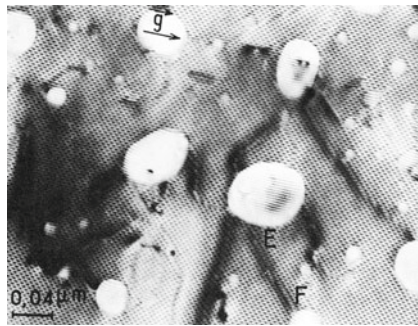


Fig. 2.7 Electronic micrograph of a low-angle twist grain boundary $\theta \approx 4^\circ$ around $\langle 001 \rangle$, in gold showing two primary screw dislocation networks aligned along the $\langle 110 \rangle$ directions (at 45° of g); the spacing between the dislocations is $d \approx 40$ nm [16]. Bubbles are artefacts (bad welded bicrystal regions) resulting from the bicrystal manufacturing; disturbed parts of the network (as EF) indicate the presence of extrinsic dislocations (see Sect. 5.2)

agree with the experiments (Fig. 2.7) [16]. As previously, other descriptions exist but their physical meaning is questionable.

It must be stressed that, whatever the chosen description of a given grain boundary, the dislocation content totally accounts for the rotation between the crystals: these dislocations are geometrically necessary. But the adopted grain boundary structure depends on the relaxations, and only the observation enables to specify what description is physically meaningful.

Besides, the distance between the dislocations decreases as the misorientation increases and becomes so small that it is no longer compatible with the crystal lattice periodicity; the dislocation stress fields then overlap. However, the O-lattice being a continuous function of the misorientation, the primary dislocations must exist from a strict geometrical point of view. This continuity is confirmed by the observation of an electron (or X-ray synchrotron) diffraction pattern of a grain boundary plane [17]. Indeed, the periodic distribution of deformations in the plane constitutes an optic grid; by selecting a diffraction spot, an electron microscopy image of the grid may be obtained. The distance between the rows of this *rebuilt* network well satisfies Eq. (2.9).

In summary, the equation giving the total dislocation content B in a grain boundary is mathematically valid whatever the misorientation θ ; but, for high θ values, it covers the physical concept of dislocation density. Another discrete description of the grain boundary structure is then proposed which refers to the second invariant of the bicrystal, i.e. the CSL lattice.

2.3.2 Secondary Intrinsic Dislocation

As postulated by Bollmann, any grain boundary adopts as much as possible the structure of the neighbored coincidence grain boundary, provided relaxations on the form of *secondary intrinsic dislocations*. These dislocations are localized in the regions of bad fit between the two DSC lattices of the coincidence grain boundary θ_c rotated one with respect to other by an angle equal to the angular deviation between the real and the coincidence grain boundaries. These lines correspond to the intersections of the grain boundary plane with the walls of the O2-lattice predicted by Eq. (1.24).

The term *secondary* comes from the fact that these defects break the periodicity of the primary dislocations. They form a sub-grain boundary in the grain boundary. Then, coincidence grain boundary regions delimited by secondary dislocations constitute the grain boundary (Fig. 2.8).



Fig. 2.8 Schematic representation of the periodic arrangement of secondary dislocations (\perp) in the primary network (\perp)

Conversely to the plurality of the primary dislocation structures for a given grain boundary, only one secondary dislocation structure is predicted by Eq. (1.24). Indeed, whatever the equivalent rotations chosen for the real and the coincidence grain boundaries, the angular deviation matrix D is identical. However, different structures may exist for non-mathematical reasons, linked to the atomic relaxations in the boundary.

The characteristics of the secondary dislocations depend on the tilt/twist character of the deviation to the coincidence. In a tilt grain boundary, a pure tilt deviation may exist either around the fundamental rotation axis or around another axis; otherwise

the deviation may have a twist or mixed character. Depending on the case, the grain boundary structure is constituted of only one secondary edge dislocation network or of two screw dislocation networks or even several mixed dislocation networks. Similarly, a twist grain boundary may present a twist, tilt or mixed angular deviation to the coincidence. In any case, the dislocation lines correspond to the intersections of the grain boundary plane with the O2-lattice walls.

The Burgers vectors of the secondary dislocations belong to the DSC lattice, but are not necessarily the elemental vectors of this lattice. In order to determine the Burgers vector of a secondary dislocation, a closed circuit drawn around the defect in the grain boundary must be reproduced in the DSC lattice of the nearest coincident grain boundary. A construction very useful for analysing the high-resolution transmission electron microscopy images enables to determine the dislocation Burgers vector and its associated step (Fig. 2.9) [18]. A secondary dislocation provokes a translation of the CSL lattice. A step vector \mathbf{s} may be defined, that relates an initial coincidence node to the coincidence node obtained by translation. If the crystal I is fixed and the crystal II translated, then the step \mathbf{s}_I is defined in the coordinate system of crystal I; and reciprocally for \mathbf{s}_{II} if the crystal II is fixed. There are several choices for the step vectors, related to each other by a DSC vector; the shortest one is usually chosen. The height of the step associated to the dislocation is $h_I = \mathbf{s}_I \cdot \mathbf{n}$ in crystal I and $h_{II} = \mathbf{s}_{II} \cdot \mathbf{n}$ in crystal II. It follows that:

$$\begin{aligned} \mathbf{b} &= \mathbf{s}_I - \mathbf{s}_{II} \\ h &= \mathbf{n}(\mathbf{s}_I + \mathbf{s}_{II})/2 \end{aligned} \quad (2.14)$$

where \mathbf{n} is the normal to the grain boundary plane (pointed from crystal I to crystal II).

The Burgers vectors of the secondary dislocations must be necessarily indexed in the reference system of the bicrystal translation lattice (the DSC lattice). Otherwise, if each vector \mathbf{s}_i is indexed in the reference system of crystal i , we obtain the primary Burgers vector of the defect.

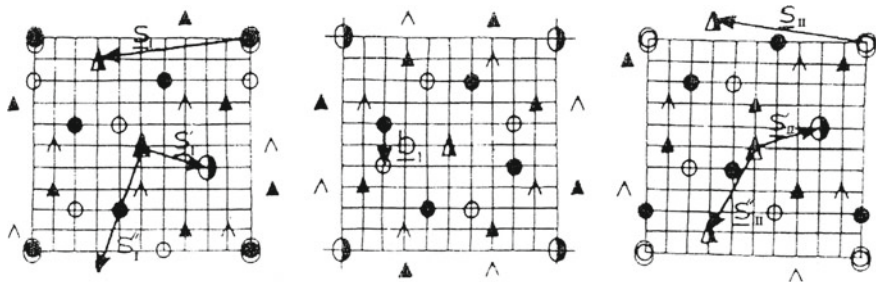


Fig. 2.9 Construction in the DSC lattice of a $\Sigma = 5$ grain boundary of three possible steps \mathbf{s} , \mathbf{s}' and \mathbf{s}'' associated to a dislocation with vector $\pm \mathbf{b}_1$. The empty and full symbols correspond to crystal II and crystal I, respectively; the *triangular symbols* represent sites located at $\pm a/2$ [100] along the projection axis; **a** CSL in its original position; **b** Displacement of crystal II relative to crystal I by a vector $+\mathbf{b}_1$; **c** displacement of crystal I relative to crystal II by a vector $-\mathbf{b}_1$ [18]

The average distance between the secondary dislocations is given by a formula similar to (2.9)

$$d = \frac{|b_{\text{DSC}}|}{2\sin\Delta\theta/2} \quad (2.15)$$

This distance decreases when the coincidence index increases ($|b_{\text{DSC}}|$ decreases) and/or when the angular deviation $\Delta\theta$ to the coincidence increases. As a result, the dislocations cannot be experimentally distinguished beyond a certain Σ value or beyond a certain $\Delta\theta$ deviation from the neighbouring coincidence relationship. Furthermore, with the diminution of $|b_{\text{DSC}}|$, the contrasts associated to dislocations in transmission electron microscopy decreases. Thus, while preserving an almost constant spacing, the dislocations are less and less visible when Σ increases. Figure 2.10 illustrates this effect for a series of $\langle 001 \rangle$ twist grain boundaries in gold [19].

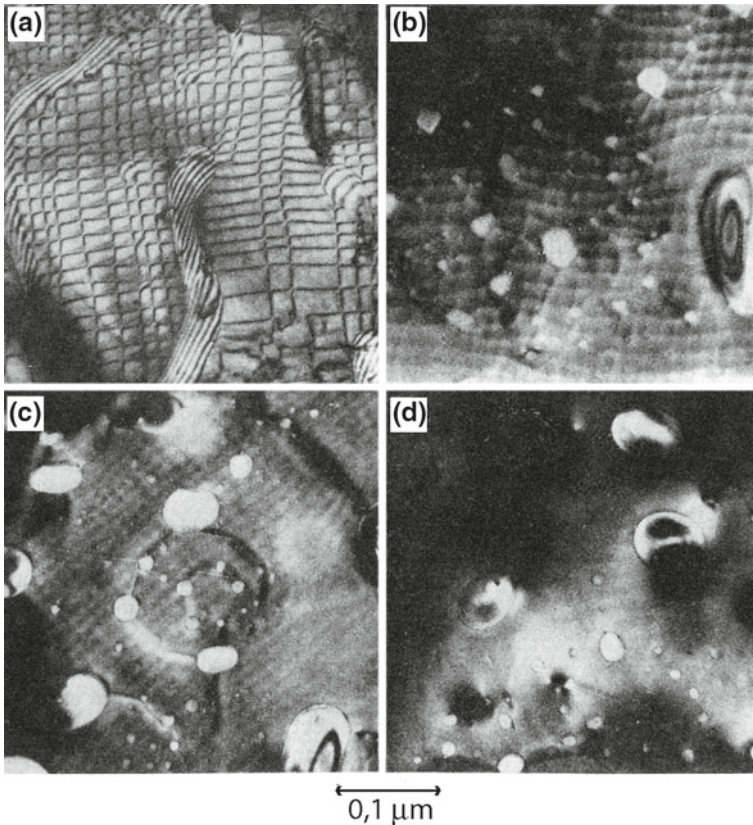


Fig. 2.10 Intrinsic secondary dislocation networks in $\langle 001 \rangle$ twist grain boundaries in gold showing the diminution of their contrast when Σ increases: **a** $\Sigma = 1$, $b = 0,289$ nm; **b** $\Sigma = 5$, $b = 0,129$ nm; **c** $\Sigma = 13$, $b = 0,080$ nm; **d** $\Sigma = 17$, $b = 0,070$ nm [19]

Figure 2.11 presents a network of secondary dislocations in a tilt grain boundary in nickel that totally account for the deviation $\Delta\theta = 0,09^\circ(112)$ of this boundary with respect to the $\Sigma = 3 \{111\}$ coincidence grain boundary [20]. Dislocations A are parallel to the $\langle 112 \rangle$ direction, their Burgers vector is the DSC vector of $\Sigma = 3$ normal to the grain boundary plane, $b = a/3 \langle 111 \rangle$, and their distance (≈ 130 nm) is in good agreement with the calculated distance.

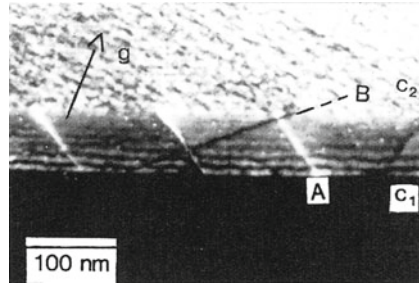


Fig. 2.11 Electronic micrograph in dark field (crystal C2 is in extinction condition) showing a network of intrinsic secondary dislocations (as A) in a near $\Sigma = 3 \{111\}$ tilt grain boundary in nickel (B is an extrinsic dislocation that will be analysed in part II, Chap. 5) [20]

The *near one-dimensional coincidence* grain boundaries displays a network of secondary dislocations, the lines of which being parallel to the intersections of the crystal planes in good fit with the grain boundary plane.

In an approximate coincidence grain boundary, the structure in terms of dislocation must account for the rotation and the deformation necessary to bring in coincidence two multiple cells of the crystals. According to the choice of the rational value of the $(c/a)^2$ ratio that approximates the real value, these two components (rotation and deformation) differ. Only the observed intergranular structure enables to specify the relaxation mode chosen by the grain boundary. Let us consider a grain boundary near the rhombohedral twin, often observed in alumina or hematite polycrystals. When the grain boundary plane is strictly parallel to the $\{01\text{-}12\}$ twin plane, the grain boundary is described by an exact bi-dimensional coincidence. But, most often, the observed grain boundary deviates from $\{01\text{-}12\}$. Then, the grain boundary is described in terms of tri-dimensional approximate coincidence, by reference to specific rotations θ around $(02\text{-}21)$ associated to rational values of $(c/a)^2$ as close as possible of the real value, $(2.730)^2$ for alumina. The specific rotations with their corresponding deformations ε for alumina are (Table 2.1) [21]:

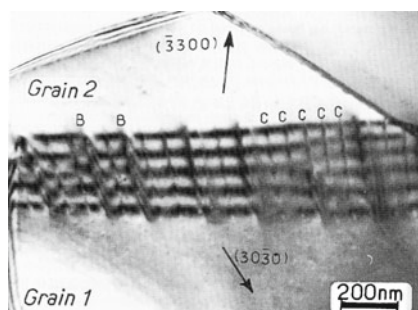
Table 2.1 Specific rotations and associated deformations giving rise to rational coincidences for rational values of the c/a ratio [21]

Σ	c/a	θ°	ε
7	2.739	85.90	0.003
29	2.728	86.05	0.001
36	2.730	86.02	0

The deformations decrease when Σ increases, this is also true for hematite ($c/a = 2,733$). Among the three previous descriptions, which is the one adopted by the grain boundary: high coincidence index ($\Sigma = 36$) and zero deformation or small coincidence index ($\Sigma = 7$) at the expense of a deformation? Only the experiment enables to answer the question.

The DSC vectors of the different descriptions are such that the intensities of two of them, \mathbf{b}_2 and \mathbf{b}_3 , are almost identical whereas the third vector \mathbf{b}_1 decreases as Σ increases. A secondary dislocation network may be observed in a grain boundary, the misorientation of which being close to that of the rhombohedral twin in alumina ($\theta = 85^\circ 5'$); the grain boundary plane is deviated by 8° from the rhombohedral plane (Fig. 2.12). The Burgers vector of the intrinsic dislocations have been identified as a linear combination of the two almost identical vectors (\mathbf{b}_2 and \mathbf{b}_3), whatever the grain boundary description. In that case, no approximate coincidence description seems to be preferred. However, in a grain boundary with a plane very close $\{01\text{-}12\}$ in hematite, the secondary dislocations, observed by high-resolution transmission electron microscopy, possess a Burgers vector that is the smallest DSC vector corresponding to a $\Sigma = 7$ coincidence relationship [22].

Fig. 2.12 Network of intrinsic secondary dislocations C in a grain boundary near the rhombohedral twin in alumina [21] (Extrinsic dislocations B will be described in part II)



In the $\theta = 90^\circ$ (10-10) grain boundaries that are numerous in tungsten carbide of hexagonal symmetry, the secondary dislocations have Burgers vectors of the $\Sigma = 2$ coincidence relationship with a deformation equal to 0.024 whereas another neighbored description with a $\Sigma = 39$ coincidence index only requires a 0.0016 deformation [23]. Similar conclusions have been obtained for the (01-12) twin in zinc of hexagonal structure. To decide what approximate coincidence is better adapted to the grain boundary structure, the dislocation lines are determined; they correspond to the intersections of the grain boundary plane with the O2-lattice associated to the smallest coincidence index, $\Sigma = 13$ in this case. But the description requires a non-negligible deformation, about 0.5 % [24].

Thus, in non-cubic system, the structure of a grain boundary close to different approximate coincidences seems to adopt that of a grain boundary with a specific rotation corresponding to the rational coincidence with the smallest index at the expense of a larger deformation of the coincidence cell.

2.3.3 Interest and Limit of the Intrinsic Dislocation Model

To sum up, intrinsic primary dislocations with Burgers vectors of the crystals describe the low-angle grain boundary structures. Similarly, a high angle coincidence grain boundary only contains primary dislocations, but the close spacing of these dislocations does not give them any physical reality. Finally, a high-angle non-coincident grain boundary contains primary dislocations accounting for the nearest coincidence structure and secondary dislocations that accommodate the deviation between the real and the coincidence grain boundaries. Most often, only the secondary dislocations are visualized as the distances between the primary dislocations are too small.

Figure 2.13 shows the evolutions of the expected dislocation spacing in function of the misorientation angle θ and in function of the deviation $\Delta\theta$ from different coincidences for $\langle 001 \rangle$ symmetrical tilt grain boundaries in gold [25]. The points reported on the curves indicate the spacing experimentally determined on the conventional transmission electron microscopy images. The smaller the coincidence index, the larger the deviation $\Delta\theta$ authorized to visualize secondary dislocations.

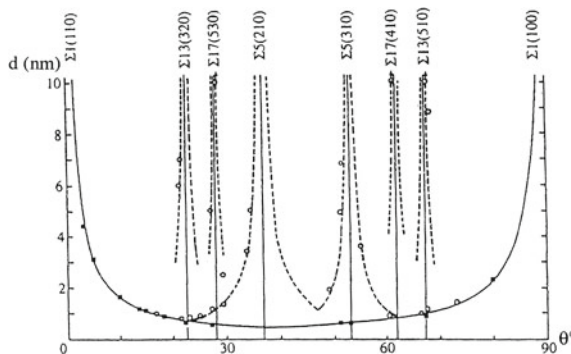


Fig. 2.13 Evolution of the spacing d (in nm) in function of the misorientation θ of the dislocations in $\langle 001 \rangle$ symmetrical tilt grain boundaries in gold. The full line and the dotted lines give the spacing of the primary and secondary dislocations, respectively. The points indicate in which grain boundaries periodic dislocations have been observed [25]

The possibilities to simultaneously observe primary and secondary dislocations are limited to few experiments; it was the case in gold for a $[001]$ tilt grain boundary deviated from about 1° from the nearest coincidence $\Sigma = 13 \{320\}$ (Fig. 2.14). The primary dislocations with Burgers vector $a/2 [110]$ are distant from 0.77 nm (calculated distance 0.75 nm) and the secondary edge dislocations with DSC Burgers vector $a/13 [320]$ are distant from 7 nm, in agreement with the theoretical distance of 7.1 nm [25].

The Bollmann formalism does not claim to describe the physical reality of a grain boundary, but constitutes a possible approach to knowledge. Bollmann himself insists that the use of the 0-lattices only permits a discrete selection of the possible

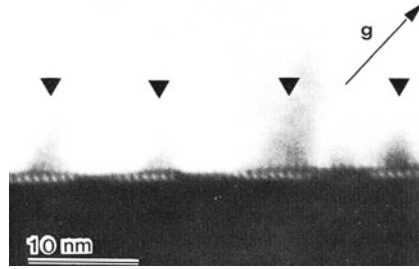


Fig. 2.14 Electronic micrograph of a symmetrical [001] tilt grain boundary near $\Sigma = 13 \{320\}$ in gold ($g = 200$). The fine periodic contrasts are due to primary dislocations with Burgers vector $a/2 [110]$, the large contrasts (*arrows*) are attributed to secondary dislocations with Burgers vector $a/13 [320]$ [25]

displacement vectors \mathbf{B} , characteristic of the continuous displacement field of the transformation \mathbf{A} . It is a first approximate model of linear relaxation in the grain boundary plane where the fact that it is linear is pure convenience.

Moreover, whatever the expression used to describe the grain boundary structure in terms of dislocations, Burgers vector density according to Frank-Bilby or discrete dislocations according to Bollmann, there are a large number of transformations \mathbf{S} (or \mathbf{R}) equivalent because of the symmetry operations of the crystals, i.e. depending on the choice of the unit cell in the reference coordinate lattice. An example has been given for the low-angle [011] tilt grain boundary (see Sect. 2.3.1). The equivalent matrices are obtained by multiplying \mathbf{S}_I , \mathbf{S}_{II} or \mathbf{R} by a uni-modular matrix \mathbf{U} corresponding to an operation of the point group symmetry of lattices I or II. Thus, there are a very large number of possible descriptions of the structure of a given grain boundary. Bollmann favours a particular description called NNR for *Nearest Neighbour Relationship* that corresponds to the minimal dislocation density by arguing that it must be associated to an energy minimum (E proportional to b^2) [26]. This argument is based on the consideration of the long-range elastic strain fields, but the local distortions due to intrinsic dislocations cancel at large distance. A grain boundary at equilibrium only generates short-range strains; the strain distribution depends on the intergranular relaxation modes and cannot be predicted by a geometrical model. The Frank-Bilby and Bollmann equations are disconnected from the grain boundary energy. Finally, a grain boundary is a unique physical object with a precise structure and a precise energy. Among all the possible structures, none can be selected *a priori*. This question will be discussed more thoroughly in the description of grain boundaries constrained at triple junctions (see Sect. 10.2.2) where it takes a particular importance.

Despite its geometrical nature, the Bollmann model has been successfully applied to identify intrinsic dislocations in numerous grain boundaries in different types of materials. It is especially remarkable that periodic dislocations have been observed, by high-resolution transmission electron microscopy, in symmetrical tilt grain boundaries with high coincidence indices, as $\Sigma = 337$ in silicon; in that case,

the Burgers vectors of the intrinsic secondary dislocations do not correspond to the elemental DSC vectors [27].

A dislocation network always reveals the existence of a preferred ordered state of the grain boundary, whatever its description. The reason why a preferred state exists is a subject of questioning in solid-state physics.

However, the high-coincidence index grain boundaries displaying periodic dislocations are not true general grain boundaries; they generally display misorientations around axes with simple indices and possess symmetrical grain boundary planes. What happens for grain boundaries with random misorientations and asymmetrical high index planes? These grain boundaries do not present dislocation networks at the scale of the conventional electron microscopy and are not observable by high-resolution electron microscopy. Do they obey a discrete or continuous description? A partial answer to this question has been advanced when we deal with the grain boundary structure at high temperature (See Sect. 4.1), then with relaxation phenomena of non-equilibrated grain boundaries (See Chap. 9).

In summary, the dislocations predicted by Eqs. (1.23) and (1.24) are geometrically necessary, but the actual dislocation content depends on the local intergranular stress relaxations. The structure is governed by the energy minimization and any forecast based on geometry alone cannot reflect reality. It is physics that determines the real mode of relaxation and a physical description requires an atomistic approach (Chap. 3).

2.4 Partial Intergranular Dislocations

The grain boundaries may also contain partial dislocations, generally associated to rigid body translations τ , thus not predicted by the geometrical formalism. Although non-periodic, these dislocations belong to the grain boundary structure [28]. Their Burgers vectors are determined by using the *circuit mapping* method proposed by Pond [29]. This circuit is analogous to a Frank circuit but is drawn in the dichromatic complex; it takes into account all the symmetry operations of the space group and not only the translations. Partial dislocations may also result from the existence of grain boundary structure variants. If regions of different structures along the grain boundary are related by a symmetry operation, they are energetically degenerate. Partial dislocations separating such regions have been observed in germanium [30] and in a copper–silicon alloy [31]. Partial dislocations are often located at the junction between two boundary facets, but may be also present in a straight part of the grain boundary. They may result of the decomposition of the DSC intrinsic dislocations, as observed in a $\Sigma = 3 \{211\}$ grain boundary where a perfect dislocation with Burgers vector $a/3 \langle 111 \rangle$ dissociates into two products with Burgers vectors $a/9 \langle 111 \rangle$ and $2a/9 \langle 111 \rangle$ [28].

2.5 Stress Fields Associated to Intrinsic Dislocations

The stress field of a low-angle grain boundary has been calculated by Hirth and Lothe, using isotropic linear elasticity and by adding the stress fields of the periodic dislocations [32]. The dislocations are mixed; three components of their Burgers vector (b_x b_y b_z) and thus three periodic networks are considered (Fig. 2.15).

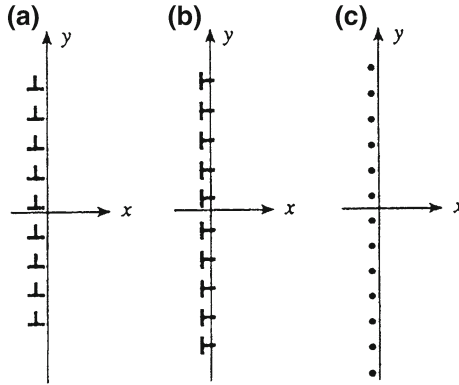


Fig. 2.15 The three periodic networks of dislocations that are considered to calculate the elastic stress fields of a low angle grain boundary. The Burgers vector of the mixed dislocations is decomposed in two edge components along Ox (a), Oy (b) and one screw component along Oy (c) [32]

For a *symmetrical tilt grain boundary* constituted of edge dislocations with Burgers vector b_x , parallel to the z axis and distant from D along Oy (Fig. 2.15a), the stress components (in regions such as $x \gg D/2\pi$) exponentially decrease with the distance x from the grain boundary ; on the contrary the stress field of an isolated dislocation is inversely proportional to the distance from its line. The expressions of the shear component σ_{xy} for the two types of defects may be compared:

- for a dislocation

$$\sigma_{xy} = \frac{\mu b}{2\pi(1-\nu)} \frac{x(x^2 - y^2)}{(x^2 + y^2)^2} \quad (2.16)$$

- for a tilt grain boundary

$$\sigma_{xy} = \frac{\mu b}{(1-\nu)} \frac{2\pi x}{D} \exp \frac{-2\pi x}{D} \cos \frac{2\pi y}{D} \quad (2.17)$$

where, μ is the shear modulus and ν the Poisson coefficient.

The expression of σ_{xx} for the grain boundary is similar to that of σ_{xy} with $\sin 2\pi y/D$ instead of $\cos 2\pi y/D$. The value of $x = 2D$ ($y = 0$), the shear component of σ_{xy} due to the periodic arrangement, is about 1 % of its value for an isolated dislocation. In the grain boundary plane ($x = 0$) and for distances $y < D/2\pi$ of a given

dislocation in the network, more than 90 % of the grain boundary stress σ_{xx} is due to the dislocation at the origin. Midway between the two dislocations, the compression stress of one dislocation is annihilated by the tension stress of the other. Then, there is no long-range stress field induced by a symmetrical tilt grain boundary. If now we consider the stress field due to a network of edge dislocations with a Burgers vector b_y (Fig. 2.15b), the component σ_{yy} does not cancel at long distance, in contradiction with the equilibrium condition given by Eqs. (2.3) or (2.4). The equilibrium of the grain boundary imposes that there is no total Burgers vector parallel to the grain boundary plane associated to edge dislocations. For the last component of the Burgers vector b_z (Fig. 2.15c), the dislocations have a twist character. For a uni-dimensional arrangement of dislocations parallel to Oz, the shear component σ_{yz} exponentially tends to zero with the distance to the grain boundary, but the stress component σ_{xz} preserves non-negligible values at large distance. A simple arrangement of screw dislocations is then incompatible with the equilibrium condition (2.4). Equilibrium in a pure twist grain boundary requires the formation of two screw dislocation networks perpendicular to each other that result in a rotation around the normal x ; the stress fields of these networks annihilate.

More generally, three dislocation networks with non-coplanar Burgers vectors account for the misorientation of a random grain boundary. For a grain boundary that satisfies the Frank-Bilby formula, the elastic stress field analysis shows that the combination of the three stress fields yields their annihilation, even if one of the network generates long-range stresses. In the calculation, the elastic constants of the crystals are used, whereas the elastic constants of the grain boundary may differ from those of the crystals as found by simulation [33]. Although the elastic constant tensor of a boundary is not known, these constants may strongly vary in the grain boundary plane [34].

Another model for calculating the stress fields is based on the grain boundary description in terms of disclinations [35]. On the contrary to the dislocation model, it takes into account the disclination core energy and may apply to high-angle grain boundaries (see Sect. 3.5).

More complex situations than those previously described by Hirth and Lothe have been addressed, in particular by considering no strictly periodic networks and by studying the evolution of their stress fields during return to periodicity. These approaches will be detailed in part II, Chap. 9 when dealing with the return to equilibrium of a non-equilibrated grain boundary.

To conclude, the knowledge of the elastic contribution is insufficient to account for the intergranular energy, we must know the contribution of the grain boundary core. This constitutes the subject of the next session focussing on the grain boundary atomic order.

References

1. F.C. Frank, *Symposium on the Plastic Deformation of Crystalline Solids* (Office of Naval Research Pittsburgh, Pennsylvania, 1950), p. 150
2. B.A. Bilby, *Report on the Conference on Defects in Crystalline Solids* (The Physical Society, London, 1955), p. 123
3. E. Kröner, in *Statistical Continuum Mechanics* (Springer, Berlin, 1972)
4. E. Kröner, in *Physics of Defects*, ed. by R. Balian, M. Klemann et J. Poirier (North Holland, Amsterdam, 1981), p. 219
5. W. Bollmann, *Crystal Defects and Crystalline Interfaces* (Springer, Berlin, 1970)
6. Bollmann, in *Crystal Lattices, Interfaces, Matrices: An Extension of Crystallography* ed. by W. Bollmann (1982)
7. W.T. Read, W. Shockley, *Phys. Rev.* **78**(195), 275 (1950)
8. A.P. Sutton, R.W. Balluffi, *Interfaces in Crystalline Materials* (Clarendon Press, Oxford, 1995)
9. G.B. Olson, M. Cohen, *Acta Metall.* **27**, 1907 (1979)
10. R. Bonnet, *J. Phys.* **43**, C6–215 (1982)
11. R. Bonnet, *Phil. Mag.* **A51**, 51 (1985)
12. D. Wolf, *Scripta Metall.* **23**, 1713 (1989)
13. P. Lacombe, L. Beaujard, *J. Inst. Metals* **74**, 1 (1947)
14. H.E. Vogel, E.E. Thomas, *Phys. Rev.* **90**, 489 (1953)
15. S. Lartigue, communication personnelle (1980)
16. L. Priester, R.W. Balluffi, *J. Microsc. Spectrosc. Electr.* **4**, 615 (1979)
17. S.L. Sass, T.Y. Tan, R.W. Balluffi, *Phil. Mag.* **31**, 559 (1975)
18. A.H. King, D.A. Smith, *Acta Cryst.* **36**, 335 (1980)
19. T. Schober, R.W. Balluffi, *Phil. Mag.* **21**, 109 (1970)
20. S. Poulat, B. Décamps, L. Priester, *Phil. Mag. A* **77**, 1381 (1998)
21. H. Grimmer, R. Bonnet, S. Lartigue, L. Priester, *Phil. Mag. A* **61**, 493 (1990)
22. L. A. Bursill, R.L. Withers, *Phil. Mag. A* **40**, 213 (1979)
23. J. Vicens, E. Laurent-Pinson, J.L. Chermant, G. Nouet, *J. Phys.* **49**, C5–271 (1988)
24. A.H. King, F.R. Chen, *Phil. Mag. A* **57**, 431 (1988)
25. E.P. Kwan, R.W. Balluffi, *Phil. Mag. A* **56**, 137 (1987)
26. W. Bollmann, *Mat. Sci. Eng.* **A113**, 129 (1989)
27. J. Thibault, J.L. Putaux, A. Jacques, A. George, H.M. Michaud et X. Baillin, *Mat. Sci. Eng.* **116A**, 93 (1993)
28. R.C. Pond, *Proc. R. Soc. Lond. A* **357**, 471 (1977)
29. R.C. Pond in *Dislocations in Solids*, vol. 8, ed. by F. Nabarro (North Holland, Amsterdam, 1989), pp. 1–66
30. J.J. Bacmann, G. Sylvestre, M. Petit, W. Bollmann, *Phil. Mag. A* **43**, 189 (1981)
31. C.T. Forwood, L.M. Clarebrough, *Phil. Mag.* **47**, 135 (1983)
32. J.P. Hirth, I. Lotte, *Theory of Dislocations*, 2nd edn. (McGrawHill, New York 1968), p. 671
33. D. Wolf, J.F. Lutsko, *J. Mater. Res.* **6**, 1427 (1989)
34. A. Aber, J.C. Bassani, M. Khanta, V. Vitek, G.J. Wang, *Phil. Trans. Roy. Soc.* **A339**, 555 (1992)
35. V.Y. Gertsman, A.A. Nazarov, A.E. Romanov, R.Z. Valiev, V.I. Vladimirov, *Phil. Mag.* **A59**, 1113 (1989)



<http://www.springer.com/978-94-007-4968-9>

Grain Boundaries

From Theory to Engineering

Priester, L.

2013, XXII, 442 p., Hardcover

ISBN: 978-94-007-4968-9